Published in final edited form as:
Methods Mol Biol. 2009 ; 489: 213–242. doi:10.1007/978-1-59745-543-5_10.

Tactile and non-tactile sensory paradigms for fMRI and neurophysiologic studies in rodents

Basavaraju G. Sanganahalli[1,3,4], **Christopher J. Bailey**[1,4,5], **Peter Herman**[1,3,4,6], and **Fahmeed Hyder**[1,2,3,4]

[1]Department of Diagnostic Radiology Yale University, New Haven, Connecticut, USA

[2]Department of Biomedical Engineering, Yale University, New Haven, Connecticut, USA

[3]Department of Quantitative Neuroscience with Magnetic Resonance (QNMR), Yale University, New Haven, Connecticut, USA

[4]Department of Magnetic Resonance Research Center, Yale University, New Haven, Connecticut, USA

[5]Center of Functionally Integrative Neuroscience, Aarhus University, Aarhus, Denmark

[6]Institute of Human Physiology and Clinical Experimental Research, Semmelweis University, Budapest, Hungary

Abstract

Functional magnetic resonance imaging (fMRI) has become a popular functional imaging tool for human studies. Future diagnostic use of fMRI depends, however, on a suitable neurophysiologic interpretation of the blood oxygenation level dependent (BOLD) signal change. This particular goal is best achieved in animal models primarily due to the invasive nature of other methods used and/or pharmacological agents applied to probe different nuances of neuronal (and glial) activity coupled to the BOLD signal change. In the last decade, we have directed our efforts towards the development of stimulation protocols for a variety of modalities in rodents with fMRI. Perception of the natural world relies on the formation of multi-dimensional representation of stimuli impinging on the different sensory systems, leading to the hypothesis that a sensory stimulus may have very different neurophysiologic outcome(s) when paired with a near simultaneous event in another modality. Before approaching this level of complexity, reliable measures must be obtained of the relatively small changes in the BOLD signal and other neurophysiologic markers (electrical, blood flow) induced by different peripheral stimuli. Here we describe different tactile (i.e., forepaw, whisker) and non-tactile (i.e., olfactory, visual) sensory paradigms applied to the anesthetized rat. The main focus is on development and validation of methods for reproducible stimulation of each sensory modality applied independently or in conjunction with one another, both inside and outside the magnet. We discuss similarities and/or differences across the sensory systems as well as advantages they may have for studying essential neuroscientific questions. We envisage that the different sensory paradigms described here may be applied directly to studies of multi-sensory interactions in anesthetized rats, en route to a rudimentary understanding of the awake functioning brain where various sensory cues presumably interrelate.

Address correspondence and reprint requests to: Fahmeed Hyder / Basavaraju G. Sanganahalli Tel: +1-203-785-6205 N143 TAC (MRRC), 300 Cedar Street Yale University New Haven, CT 06510, USA Fax: +1-203-785-6643 fahmeed.hyder@yale.edu / basavaraju.ganganna@yale.edu.

Keywords

anesthesia; awake; blood flow; metabolism; neuroimaging; tactile

2. Introduction

Dynamic imaging of human brain function began approximately two decades ago with positron emission tomography (PET) (for reviews see [1,2]). Since the 1990s, however, nuclear magnetic resonance (NMR) – both imaging (MRI) and spectroscopy (MRS) – has played a major role in studies of *in vivo* neuroscience, both in animals and humans (for reviews see [3,4]). The discovery of functional MRI (fMRI) by Seiji Ogawa in 1990 [5] further reinforced the role of functional imaging studies in neuroscience. The fMRI method, as originally proposed, depends on the paramagnetic effect of deoxyhemoglobin (in blood) upon the NMR transverse relaxation times of nearby water protons (in tissue) [6]. Since changes in the oxygen level in the blood determine the fraction of deoxygenated hemoglobin, the image contrast was fittingly termed blood oxygenation level dependent (BOLD).

After the initial demonstrations of the BOLD method in mapping dynamic brain function in humans during sensory stimulation [7–10], the cognitive neuroscience community immediately embraced the method [11]. Today BOLD fMRI is arguably the most popular functional mapping tool for human studies, perhaps in part due to its non-invasive nature of application, relatively good spatiotemporal resolution, superior coverage of large parts of the brain, and the fact that experiments can be conducted on most clinical MRI scanners by slight adjustments. However future utility of fMRI for diagnostic and treatment measures in humans is largely dependent on a better neurophysiologic interpretation of the BOLD signal change because the conventional fMRI map reflects changes in blood oxygenation, not the actual neuronal activity [12–14]. This particular goal seems to be best achieved in animal models [15–17] primarily due to the invasive nature of the non-NMR methods used [18–20] and/or pharmacological agents applied [21–23] to probe different features of cellular activity coupled to the BOLD signal change.

In the last decade, we have invested considerable research efforts towards developing various sensory stimulation protocols in rodents with fMRI [24–26]. Over that same period of time, coupled with state-of-the-art NMR advancements in high magnetic field scanners and improvements in other hardware components (e.g., gradient, shim, and radio frequency coils) [27], we are now able to reproducibly [28,29] measure relatively small BOLD signal changes (in rat or mouse brains) induced by peripheral stimuli with superior spatiotemporal resolution [30,31]. Here we describe tactile (i.e., whisker, forepaw) and non-tactile (i.e., olfactory, visual) sensory paradigms applied to the anesthetized rat. We discuss features of peripheral stimulus delivery equipment needed to generate identical stimuli, both inside and outside the magnet. The focus is on development and validation of methods for stimulation of each sensory modality applied independently or in conjunction with one another. We demonstrate reproducibility of induced activations, as measured by changes in BOLD signal and other non-NMR signals (e.g., electrical activity, laser-Doppler blood flow), achieved with different sensory paradigms and discuss similarities and/or differences across the different sensory systems as well as the potential advantages they may have for the study of different neuroscientific questions.

The mammalian brain functions in a world full of sensory cues. The nature of stimuli perturbing the different sensory domains is quite diverse – from odorant molecules at the nose epithelium and photons bombarding the retina, to sound vibrations of the eardrum and

mechanoreceptors on the skin. As a consequence, the brain structures dedicated to different senses are anatomically distinct, from the level of cell types to their vast synaptic interconnections [32]. Therefore different peripheral stimuli of the rodent brain offer a rich platform on which to test effects of perturbations on functionally and anatomically heterogeneous populations of neural tissues. In addition, the vast literature on rodent brain anatomy, morphology, and physiology make possible viable extrapolation of results from such experiments.

Since the physical world around any creature impinges on all its sensory systems in parallel, a multi-dimensional representation of the surroundings is thereby needed for complex (e.g., hunting for prey) and even simple (e.g., avoidance of noxious conditions) behaviors. A central hypothesis in design of the controlled fMRI and neurophysiologic studies, as described here and executed similarly in many other laboratories around the world, is that sensory stimuli may have very different neurophysiologic outcome(s) when paired with a near simultaneous event in another modality. The different sensory paradigms described here may be applied directly to the study of multi-sensory interactions in anesthetized rats [33] and elucidation of such effects with high spatiotemporal precision is hypothesized to contribute to the understanding of the awake functioning brain [34].

3. Materials and methods

The design principle of our approach for reproducible stimulation of multiple senses can be summarized with the word *modularity*. The different sensory systems we aim to probe clearly necessitate specialized stimulus delivery solutions, operating at appropriate timescales. However care was taken not to build mutually exclusive apparatus for the different senses (i.e., one stimulus modality should not prevent concurrent or simultaneous application of another). The basic requirement of accurate dynamic control over the stimuli called for computerized implementation. Therefore all of our designs are based on a CED μ1401 analog-to-digital converter unit (or CED unit), in particular its programmable analog and digital output capabilities, controlled by custom-written scripts running in Spike2 environment (Cambridge Electronic Design, Cambridge, UK) on standard personal computers. All wires, pipes, and optical fibers needed to deliver the stimuli to the rodent were led into the magnetically shielded scanner room through small access holes in the sidewall. Exactly the same stimulus delivery mechanisms were applied to the rodents outside the magnet for bench neurophysiologic studies. All of the stimulation devices described below were home-built.

3.1 Stimulation devices

Olfactory stimulator—The design of the olfactometer is based on John Kauer's original idea [35]. We follow the design implemented in Lawrence Cohen's laboratory [36] but with specific modifications necessitated by the long delivery conduits needed between odorant source (outside the magnet room) and the subject (inside the magnet). Our olfactometer was designed and built to control the delivery of odorants mixed in air provided by an aquarium air pump. A schematic of the design is shown in Fig 1. A charcoal filter was used to remove odorants present in room air, before entering a system of solenoid valves (2 inlets and 1 outlet; Cole-Parmer Instrument, Vernon Hills, IL) and acrylic flow meters (maintained at 1 L/min; Cole-Parmer Instrument). The output of the flow meters was connected to long (~8 m) Teflon tubes that were led into the scanner room and then connected to a glass tube placed in front of the rat lying inside the magnet bore. The state of each solenoid valve (open/closed) was switched using a relay circuit, controlled by the CED unit using Spike2 software. To provide a continuous steady-state environment to the nasal mucosa, the applied airflow was humidified and preheated to 28–30 °C.

The olfactometer operated as follows. Filtered air enters the first solenoid valve (S1, always open except during the odor delivery) and the connected flow meter (FM) delivers that air to the freely breathing rat. The filtered air stream also enters a glass bottle with a specific odorant, from which the output is led through the second solenoid valve (S2). The input to a third solenoid valve (S3) is connected to a vacuum pump. During odorant stimulation, S2 is opened for a defined duration, causing a constant flow of the odorant, mixed in air, to be delivered into the glass tube in front of the rat. To rapidly end the stimulus, S3 is opened for a short period of time causing a transient vacuum in the delivery tube and thus sucking out all remaining molecules of the odorant. Each solenoid valve was switched in less than 50 ms. A straightforward extension to the system described above is one with multiple odorant containers, solenoid valves, and flow meters arranged in parallel to allow mixtures of odorants to be presented.

Visual stimulator—The implemented design of the visual stimulus delivery system resulted from iterative modifications with the primary goal of being able to provide a variety of colored lights with wide ranging intensities and/or orientations while the ambient lighting inside the room or the magnet bore remained constant. Therefore our design differs from the stroboscopic-based [37] or dark-light adapted [38] systems which generate very robust intensity stimuli. The light was delivered to the rodent by polymer-based fiber optics (Fiber Optic Products, Clearlake Oaks, CA). Two thin (inner/outer diameters of 1.0/2.3 mm) polyethylene-coated optical fiber cables for independent stimulation of each eye were led into the scanner room. A home-built fiberglass platform was secured in front of the animal (outside the magnet bore) that allowed the positioning of small cradles which in turn could be rotated to ensure optimal intensities and/or orientation of light source relative to each eye. Each semi-circular cradle, angled slightly down, was designed to securely hold a cylinder into which the optical cable was fixed. The light from the cables then illuminated the back of an acrylic lens (diameter of 6.4 mm) placed inside the cylinder. A piece of paper with alternating black-and-white stripes was glued to the back of the lens so that the dispersed light exiting the cable lead to a larger viewing angle and at the same time created better spatial contrast. The method has been shown to enhance responsiveness of primary visual cells in the rat [39]. Given the distance between the illuminated lens and the eyes (i.e., ~2.3 cm), we could then estimate the angle in the visual field subtended by each stimulus. With reference to an origin at the intersection of the sagittal midline, the coronal interocular line, and the horizontal plane through the eyes, the stimuli appear approximately at 35–50° azimuth and 10–40° elevation relative to the horizontal meridian.

In addition to a spatially specific and robust stimulus delivery method, our goal was to control accurately both the intensity (lux) and wavelength (color) of the stimuli. We opted for light emitting diodes (LEDs; Luxeon Star III, Lumileds Lighting, LLC, San Jose, CA), which come in a variety of colors (i.e., with well defined emission spectra) including “white.” A power module (LuxDrive BuckPuck, LEDdynamics, Randolph, VT, USA), with a custom-made associated circuitry, was used to convert an applied voltage to a constant current fed to the LEDs because the output luminous intensity of LEDs is more linearly proportional to current. The controlling input voltage was applied by the CED unit using Spike2 software. We used acrylic collimator lenses to target the wide-angle LED light into the optical cables, which attached to cradles in front of the LEDs. The intensity of light entering each cable could thus be independently adjusted. Before each experiment, we calibrated the stimuli using a light meter (Extech Instruments, Waltham, MA). We measured, at four different pre-defined input voltages, the illuminance (in lux units) emitted from the stimuli.

Whisker stimulator—The design of our whisker stimulator is based on accurate control of airflow through solenoid valves, similar to the case of the olfactory stimulator as

discussed above. Aquarium air pumps were connected to two computer-controlled valves, the outputs of which were connected to long (~8 m) Teflon tubes that ran the length of the imaging bore to the rat's whisker pad. Whiskers on the chosen side(s) were trimmed to a length of ~20 mm. All non-stimulated whiskers, including the non-selected whiskers on the contralateral side, were trimmed away to avoid spurious activations. A lightweight masking tape (length and width of 20 and 6 mm, respectively) was fastened to the chosen whisker(s) to increase resistance to airflow while at the same time ensuring identical motion of the selected whisker(s). By alternative opening and closing of the solenoids we generated short air puffs through the tubes near the whiskers. The distance between the tubes and the whiskers was typically about 2 cm. The default orientation of the tubes moved the whiskers in a rostro-caudal direction, but dorsal-ventral is also possible by changing the orientation of the tubes relative to the whisker pad. Alternating air puffs at rates of up to tens of Hz deflected the stimulated whiskers by ~2 mm.

Forepaw stimulator—A pair of thin needle copper electrodes was inserted under the skin of the chosen forepaw(s). Square wave current pulses of 0.3 ms duration and variable amplitude (0.2–2 mA) were generated by use of an isolator unit (WPI, Sarasota, FL) connected to the electrodes. To control stimulus timing and frequency (typically 1–9 Hz), digital output signals were generated by the CED unit using Spike2 software.

3.2 Animal preparation

All procedures were performed in accordance with protocols approved by the Yale Animal Care and Research Committee. Experiments were conducted on male rats (Charles River, Wilmington, MA; fed *ad libitum*) weighing between 180 and 350 g. In all rats, a femoral artery was cannulated with a polyethylene catheter (PE-50) to withdraw blood samples for blood gas analysis and to monitor arterial blood pressure, an intraperitoneal catheter (PE-10) was inserted for administration of soluble anesthetics, and a femoral vein was cannulated with a polyethylene catheter (PE-10) to administer other drugs. Blood pressure was continuously monitored. Ventilation parameters were adjusted to maintain arterial blood gas tensions (pCO_2, pO_2, pH) within normal range. A rectal temperature probe was inserted to monitor and maintain the core body temperature at ~37 °C with a temperature-controlled re-circulated warm water pad. All monitoring equipment, consisting of magnetic materials, were placed outside the scanner room and sampled by the CED unit for online recording. A standard block stimulation protocol was used in all experiments. We monitored analgesia depth by pain response to an automated electrical (5 mA, 0.3 ms, 1 Hz, 1 s) tail-pinch every ¼ hour.

Forepaw and whisker studies—The rats (Sprague-Dawley) were initially anesthetized with 1.5–2% halothane in a mixture of 70% N_2O and 30% O_2. Tracheotomy was performed and the animal was artificially ventilated with 0.75–1% halothane in a mixture of 70% N_2O and 30% O_2 during all other surgical procedures. *D*-tubocurarine chloride (initial 0.5 mg/kg; supplemental 0.25 mg/kg/h; intravenous) was used to immobilize the rat. After all surgical procedures were completed halothane was discontinued and anesthesia was maintained with α-chloralose (initial 80 mg/kg; supplemental 40 mg/kg/h; intraperitoneal).

Visual studies—The commonly used albino strains of experimental rats, such as Sprague-Dawley, possess significantly poorer visual acuity than their wild counterparts [40]. The primary causes may be the lack of pigment in the retinal epithelium, leading to light scattering in the eye and abnormal development of retinothalamic [41,42] and interhemispheric cortical connections [42,43]. Therefore we opted for the pigmented “hooded” Long-Evans strain of rats for our visual experiments only. Preparation was similar

to forepaw and whisker studies with the exception that isoflurane was used for induction (3–4%) and surgery (1.5–2%).

Olfactory Studies—Male Sprague-Dawley rats were anesthetized with urethane (1.3 g/kg, intraperitoneal) with additional doses (0.13 g/kg, intravenous) administered if necessary depending on the duration of the experiment. These rats were freely breathing (i.e., no tracheotomy).

3.3 Experimental setup for fMRI studies

We used a custom-designed cradle with a bite bar for head immobilization during fMRI scans. All stimulus delivery items were secured onto the holder with adhesive tape. In some cases, to record electroencephalogram (EEG) simultaneously with fMRI, we used a pair of carbon fibers (WPI) placed bilaterally over the parietal cortex between the scalp and the skull [44]. All fMRI data were obtained on a modified 11.7T Bruker horizontal-bore spectrometer (Bruker AVANCE, Billerica, MA) using a ^{1}H surface coil (diameter of 14 mm) radio frequency probe. The cradle was securely placed under the coil. The z axis position was dependent on the stimulus used and distance between coil and head (y axis) was minimized.

A voxel of ~100 and ~300 μL, respectively, for the bulb and brain was shimmed with fast, automatic shimming technique by mapping along projections (FASTMAP) [45] utilizing first and second order shim gradients. The static field inhomogeneity was optimized until the half-height line width of water in the shimming voxel was less than 15 and 20 Hz, respectively, for imaging the bulb and brain. The neuroanatomy was imaged with either the rapid acquisition relaxation enhanced (RARE) [46] or fast low-angle single shot (FLASH) [47] contrast sequence. For all brain studies, we used single-shot echo-planar imaging (EPI) [48] with sequential sampling [49] and the following parameters: recycle time (TR) = 1000 ms; echo time (TE) = 15 ms; field of view (FOV) = 2.56×2.56 cm^2; image matrix = 64×64; number of slices = 3 or 6; slice thickness = 2 or 1 mm; voxel size = 320 or 160 nL; flip angle = 45–60°. For olfactory studies, we used FLASH contrast and the following parameters: TR = 500 ms; TE = 15 ms; FOV = 1.56×1.56 cm^2; image matrix = 64×64; number of slices = 20; slice thickness = 250 or 500 μm; voxel size = 15 or 30 nL; flip angle = 15–30°.

3.4 Experimental setup for electrophysiology and laser-Doppler flowmetry

The rat was placed in a stereotaxic holder (David Kopf Instruments, Tujunga, CA) sitting on a vibration-free table inside a Faraday cage adjacent to the scanner. For all somatosensory region recordings, we developed a combined dual-probe consisting of a high impedance microelectrode and a fiber optic laser-Doppler probe [50,51]. The microelectrode was glued to the side of an 18 G spinal needle shaft (Terumo, Tokyo, Japan) and the bare laser-Doppler probe was placed inside the needle shaft so that tips of each sensor protruded (approximately 1.5 mm) beyond the needle tip. The shaft of the needle was then placed in a microelectrode holder (Plastic One, Roanoke, VA) on the stereotaxic apparatus, and the tip of the dual-probe was advanced into the rat cortex (see below) to a depth corresponding to cortical layer 4, which could later be verified by histology [52]. For all olfactory bulb and visual recordings, only the microelectrode was used. The coordinates for all neurophysiologic measurements were guided by prior fMRI data [16,26].

Cerebral blood flow (CBF) was measured using a fiber optic laser-Doppler probe (830 nm; Oxford Optronix, Oxford, UK) sensitive to red blood cell flux. The bare fiber laser-Doppler probe had a total diameter of less than 450 μ-m. CBF was dynamically recorded by the CED unit without any additional filtering. Electrical activity was measured with tungsten matrix microelectrodes consisting of two electrodes separated by 410 μm (FHC, Bowdoinham,

ME) with high impedance (2–4 MΩ, tip size <1μm). The pre-amplified electrical signal was digitized with the CED unit. The data were collected with a large bandwidth (10 Hz - 20 kHz) and filtered into local field potential (LFP; 10–150 Hz) and multi unit activity (MUA; 300–1500 Hz) bands. The LFP data were represented in the raw arbitrary units of mV. From the MUA data, a template-matching algorithm (Spike2) was used to detect action potentials fired by individual neurons near the electrode tips to calculate spike rates (10 s bins) in units of Hz.

For recordings from somatosensory regions, tiny burr holes above contralateral and ipsilateral areas [forelimb area ($S1_{FL}$): 4.4 mm lateral and 1.0 mm anterior to bregma; whisker barrel field ($S1_{BF}$): 4.5 – 5.5 mm lateral 2.5 to 3 mm posterior to bregma] were thinned and the skull was carefully opened. Recordings from the visual areas were usually guided by locations from the Paxinos and Watson atlas [53]. For recordings from the olfactory bulb, tiny burr holes above the olfactory bulb were made [medial location: 0.5 mm lateral and 7.7 mm anterior from bregma; lateral location: 1.5 mm lateral and 8.7 mm anterior from bregma].

4. Results

4.1 Olfactory stimulation

We examined odorant induced activity patterns in the olfactory bulb with ester (iso-amyl acetate) and aldehyde (hexanal) stimulations given to both nostrils in the same subject (Fig. 2). None of the odorants or their concentrations examined caused any stimulation induced variations in systemic physiology (data not shown). In agreement with prior fMRI findings using a variety of odorants [26,54,55], the strongest BOLD activations were located mainly within the glomerular and olfactory nerve layers. Together these layers comprise the outermost layers of the olfactory bulb and span about 100 μ-m in the thinnest region to about 500 μ-m in the widest region of the olfactory bulb. While both iso-amyl acetate and hexanal elicited patterns with some degree of overlap in dorsal, lateral, and medial regions, hexanal generated much stronger ventral activations. In prior fMRI studies with esters and aldehydes [54,55], we found presence of ventral activations for aldehydes of different carbon lengths. For a given odorant, the activation patterns were not exactly symmetrical across the two bulbs, perhaps due to individual variations of air intake capabilities of each nostril. In all cases examined ($n = 5$), inter-bulbar asymmetries within one subject were much larger than intra-animal experimental variations. We refer to our previous studies [26,55] for extensive discussion of activation patterns in the olfactory bulb.

Due to the strong medial and lateral BOLD activations observed with hexanal, we compared the BOLD signal changes with LFP recordings in the same locations (Fig. 3). The BOLD activation maps were used to identify the lateral and medial foci (Fig. 3A,B) for the LFP recordings (Fig. 3C). The strong BOLD response during hexanal stimulation (6–10%) is in good agreement with prior fMRI results for iso-amyl acetate [56]. The LFP recordings demonstrated complicated dynamic evoked patterns that suggest multiple frequency components, ranging between 5 and 25 Hz, where latencies of both medial and lateral responses were about 1 s. While these fMRI-guided LFP results partially agree with classical LFP recordings from the olfactory bulb [57], further characterization of the LFP response is needed to distinguish between the latencies and the different frequency components [58], for different regions and/or odorants.

4. 2 Visual stimulation

We investigated light induced activity patterns in the visual areas of the brain (Fig. 4). There were no stimulation induced variations in systemic physiology for the intensities (20–40 lux)

or colors (white, green) of light examined (data not shown; $n = 4$). Bilateral, white light (50 ms pulses; 1 Hz; 30 lux) stimulation elicited reproducible bilateral BOLD activations (Fig. 4A) in the dorsal lateral geniculate nuclei of the thalamus (DLG), the primary visual cortex (V1), and the dorsal layers of the superior colliculus (SC). Both the amplitude (~2%) and locations (DLG, V1, SC) of the BOLD response are in good agreement with prior fMRI results from Long-Evans rats [37]. At higher stimulation frequencies, localized BOLD time courses from the DLG and V1 regions (Fig. 4B) revealed a weaker response in V1 and a slightly stronger response in DLG. The MUA signals from these regions were in general agreement with the fMRI findings (Fig. 4C). Results with green light (data not shown) were qualitatively similar to the results shown for white light.

4.3 Whisker stimulation

We explored whisker stimulation induced activity patterns in the somatosensory area (Figs. 5,6). There were no stimulation induced variations in systemic physiology for whisker movement frequencies of less than 40 Hz (data not shown). Rostro-caudal movement of whiskers caused by air puffs over a wide range of frequencies reproducibly stimulated the contralateral, primary somatosensory area of the whisker barrel field ($S1_{BF}$). Repeated trials in the same subject and across subjects produced activations in approximately the same locations in the contralateral $S1_{BF}$ (Fig. 5A). We observed medial to lateral extent of contralateral $S1_{BF}$ activation, presumably because many whiskers were stimulated simultaneously. Given prior information about contralateral $S1_{BF}$ activation [59–61], we hypothesize that the number of barrels corresponded approximately with the number of whiskers stimulated. The robust and reproducible contralateral $S1_{BF}$ activation was probably improved because whiskers on the ipsilateral side were clipped to remove spurious artifacts.

The averaged BOLD response with 8 Hz whisker stimulation (Fig. 5B) from the contralateral $S1_{BF}$ (~4%) was in good agreement with prior findings under similar experimental conditions [25,62]. While the BOLD response was sustained for the duration of the stimulus, the signal usually decreased towards the pre-stimulus baseline as soon as the stimulus was terminated. In the same subject, we have used 30 s and 120 s duration stimuli and observed sustained BOLD response (data not shown). Localized $S1_{BF}$ measurements of CBF (Fig. 5C) and MUA (Fig. 5D) were well correlated with the fMRI results. Increasing the stimulation frequency augmented the BOLD response in the contralateral $S1_{BF}$ (Fig. 6), where in the same subject the BOLD response for 12 Hz stimulation was nearly twice the magnitude of the response for 4 Hz stimulation.

4.4 Forepaw stimulation

We evaluated forepaw stimulation induced activity patterns in the somatosensory area (Figs. 7,8). There were no stimulation induced variations in systemic physiology for forepaw stimulation amplitudes of less than 5 mA and frequencies of less than 40 Hz (data not shown). Electrical stimulation (2 mA, 3 Hz) of the forepaw with 0.3 ms duration pulses for 30 s evoked a strong positive BOLD signal change in the contralateral, primary somatosensory area of the forelimb ($S1_{FL}$). No significant BOLD signal changes were observed in the ipsilateral $S1_{FL}$ region during unilateral forepaw stimulation. In a given subject, when either the left or the right forepaw was concurrently stimulated, there were no significant differences in the BOLD response between the two $S1_{FL}$ regions (Fig. 7A). The intra-subject reproducibility of BOLD activations with either forepaw stimulation (Fig. 7A,B) was nearly indistinguishable from the inter-subject reproducibility of BOLD activations (Fig. 7C), as assessed by the number of significantly activated pixels in the $S1_{FL}$ region and/or the averaged BOLD signal change in the $S1_{FL}$ region (data not shown). These results are in good agreement with prior fMRI observations [24,63].

The averaged BOLD response with 3 Hz forepaw stimulation (Fig. 8A) from the contralateral $S1_{FL}$ (~8%) was in good agreement with prior findings under similar experimental conditions [24,63]. The BOLD response was sustained for the duration of the 30 s stimulus (Fig. 8A) and even when the stimulus duration was lengthened to several minutes (Fig. 8B). Increasing the stimulation frequency above 3 Hz decreased the BOLD response in the contralateral $S1_{FL}$ (data not shown), which is in good agreement with prior observations [64,65]. Localized $S1_{FL}$ measurements of CBF (Fig. 8C) and MUA (Fig. 8D) were well correlated with the fMRI results.

5. Discussion

5.1 Summary of fMRI and neurophysiologic results

We demonstrated the ability to deliver four independent sensory stimuli to anesthetized rats lying inside an MRI scanner and replicated identical conditions during neurophysiologic measurements outside the scanner. Noticeably, however, evoked BOLD responses with olfactory, visual, and whisker stimuli exhibited slight variability during the stimulation period (e.g., the BOLD response in the S1BF declines), whereas forepaw stimuli demonstrated relatively stable BOLD signal change. This is most likely a reflection of the nature of forepaw stimuli in which strong and highly synchronous barrages of identical efferent inputs invade the contralateral S1FL, causing massive activity of cortical neurons, and which in turn may partially explain the larger BOLD response with the forepaw stimulation. It is unlikely that the forepaw stimulus is out of the physiological range,because the systemic physiology was unaffected by the stimulus, as observed similarly with the other stimuli. Since we could tightly control the systemic physiology (i.e., pH ≈ 7.35; pCO_2 ≈ 37 mmHg; pO_2 > 100 mmHg; blood pressure ≈ 95–110 mmHg; core temperature ≈ 37 °C) for α-chloralose anesthetized rats which were given visual, whisker, and forepaw stimuli, we did not exclude a high number of animals from our studies. However for the urethane-anesthetized rats receiving olfactory stimuli (i.e., no tracheotomy), temperature was the only parameter that could be efficiently controlled, and which unfortunately did not prove to be sufficient as we had to exclude nearly ½ of the experiments due to poor maintenance of systemic physiology. These issues are discussed further below (see 5.2).

The variable BOLD responses with different sensory inputs – which ranged from diffuse odorant maps (in the olfactory bulb) to highly localized somatosensory and visual foci (in the brain) – presumably reflected neurophysiologic variations across the sensory modalities as well as their neuroanatomic underpinnings. The localized neurophysiologic responses, measured here with the electrical (i.e., LFP or MUA) and/or the coupled CBF signal and which were in general agreement with the fMRI results, can be used to provide complimentary insights to the multi-modal basis of the BOLD signal change [12–14]. Generally the MUA responses from the brain (i.e., DLG, V1, $S1_{BF}$, and $S1_{FL}$) were quite comparable, with 5–7 Hz incremental change in ensemble firing rate for the respective stimuli. However the CBF changes in the $S1_{BF}$ was nearly ½ that observed in the $S1_{FL}$. But the time lags to reach the CBF peak were nearly identical with whisker and forepaw stimuli, whereas the CBF responses reached peak nearly ~2 s earlier than the BOLD responses.

Non-tactile: Olfactory stimulation—With the sole exception of the olfactory system, all peripheral sensory neurons synapse within domain-specific regions of the thalamus, before reaching the primary sensory cortical regions. When air containing odorant molecules is inhaled into the nasal cavities, a rich collection of receptor neurons in the olfactory epithelium (and which later comprise the outermost olfactory nerve layer in the olfactory bulb) converts the information into electrical form. As a molecule binds to a matching receptor, an impulse is sent to the olfactory bulb, which in the rodent is located just anterior

to the frontal lobe and is separated into two “identical” hemispheres each with a multi-layered organization [66]. Signals from receptor neurons arrive at the glomerular layer, where they are integrated by a large number of mitral/tufted cells that project their axons out of the olfactory bulb onto the olfactory cortex, specifically piriform and entorhinal cortices, amygdale, and the olfactory nucleus.

The olfactory bulb, more specifically the glomerular layer, has been shown to form “chemotopic maps” with exposure to specific odorants (i.e. responses to different odorants are processed in anatomically distinct locations in the glomerular space) using a variety of techniques [67–71] including fMRI [26,29,54–56,72,73]. Therefore functional mapping at the level of individual glomeruli is important and this spatial resolution is quite commonly attainable with optical imaging [58,68]. However this technical feat has also been achieved in the past with fMRI using voxel sizes less than 10 nL [74,75]. For the current studies, however, we acquired data with high BOLD sensitivity in slightly larger voxels to cover the entire bulb at a temporal resolution superior to most other whole bulb mapping techniques. Furthermore the minimally invasive approach of fMRI allowed repeated perturbations on the same subject to provide comparison across different experimental runs (from the same subject) without any averaging.

With our stimulation device we were able to test response variability to different odorants (Figs. 2,3) as well as their concentrations (data not shown). We observed diffuse BOLD responses in the bulb, where a large proportion of the bulb was active for any given odorant and the activity patterns were specific to the odorant type (Fig. 2). While we correlated LFP signals to a few medial and lateral BOLD foci (Fig. 3), understanding the complex frequency components within the LFP responses and their relationship to the BOLD response remain a future area of research. Given that fMRI can inherently detect both hemispheres simultaneously, the hypothesized “identical” function of each bulb could also be tested in the future. Since we could not vary the incident direction of the odorants with the current delivery device, plans are underway to include spatial specific delivery tubes for directional delivery inside the magnet bore. However all of these endeavors will require a next generation of fMRI hardware improvement (e.g., with parallel imaging [76,77] using multiple smaller radio frequency coils) because of the smaller BOLD responses expected.

Non-tactile: Visual stimulation—Though a predominantly nocturnal animal, the rodent makes use of its visual system when lighting conditions are favorable – e.g., for vision-based navigation [78]. Light enters the retina, which contains elongated photoreceptor cells that are full of light-sensitive photopigment molecules (or opsins). Upon interacting with incident photons, photoisomerization of rod and/or cone opsins initiates a cascade of processes that rapidly lead to a decrease in the intracellular concentration of cyclic GMP molecules, thereby changing the cell membrane's permeability to cations and thus altering its potential [79]. This graded signal is refined further by retinal networks before being transmitted, via the dorsal lateral geniculate nucleus of the thalamus, onto the primary visual cortex in the contralateral occipital lobe. A parallel pathway, bypassing the thalamus, transmits visual information to the superficial layers of the contralateral superior colliculus. The rat retina has two distinct types of cones – most sensitive to medium wavelengths (~510 nm; i.e., green) but some receptive to very short wavelengths (~360 nm; i.e., ultraviolet) – allowing discrimination between different colors [80].

Our visual stimulation setup allowed us to vary the color and/or intensity of light pulses of different durations. At a constant pulse width of 50 ms and intensity of 20–30 lux, white (Fig. 4) and green (data not shown) light evoked well-localized cortical and sub-cortical multi-modal responses which corresponded well with known retinotopic maps of both the primary visual cortex [81,82] and the superior colliculus [83]. At higher stimulation

frequencies responses weakened in V1 and strengthened in DLG. These results confirmed a previous fMRI report that examined the effect of stimulus frequency on the cortical BOLD response [37] where there is an apparent inverse relationship between increasing flash frequency and BOLD response amplitude. A limitation of our method, however, is the inability to produce moving stimuli, such as drifting gratings typically employed in studies of the visual system to map response properties of single cells [84]. Since the optimal tuning properties of cells in the rat visual cortices appear to be randomly arranged [85], the probability of recording signals from an optimally excited neuron within an ensemble is reduced. Regardless, we were able to record ensemble multi-unit discharges in the V1 and DLG and demonstrated their qualitative concurrence with the fMRI data. To relate these rat studies to results from other species where vision plays a more important role in their livelihood [15,18–20], studies are underway to examine the degree of temporal correlation between LFP, MUA, and BOLD signals in V1, SC, and DLG.

Tactile: Whisker stimulation—The rat relies heavily not only on its exquisite sense of smell, but also on its vibrissa (i.e., whisker system). On either side of its face, the rat has approximately 35 whiskers organized in a grid-like pattern of rows and columns. The roots of these are long hairs are wrapped in mechanoreceptors sensitive to minute vibrations. The signals generated by motion of the whiskers are transmitted via the trigeminal nerve to the ventral posterior lateral nucleus of the thalamus to whisker-specific regions in the primary somatosensory cortex. The conspicuous anatomical detail of densely packed clusters of cells, forming a topographic map of the contralateral whisker pads [86] led to the concept of “barrel” cortex [87]. During exploration of their environment, rats actively make contact with objects with their whiskers by voluntary head motions and facial muscle activity. The combined multi-parametric effects of the amplitude, frequency, and motion of whisker deflections upon impact provide the sensation of the object.

The whisker stimulation is a difficult model to apply reproducibly inside the magnet primarily because of space constraints. Nevertheless our prior approach for whisker stimulation inside the magnet [26,62] using Lorentz force to move a small conducting copper wire attached to the whiskers is unfortunately not easily reproduced identically outside the magnet. A good alternative is mechanical movement of whiskers [88], but this works poorly inside a magnet. Since this method requires a non-magnetic manipulator which must span the entire length of the bore, dexterity becomes a problem and therefore there is limited control of the amplitude and/or frequency of the whisker stimulation. Thus we developed a non-magnetic whisker stimulation device using air puffs which can be easily used – either simultaneously or concurrently – with almost any other sensory stimuli (e.g., forepaw, olfactory, visual), both inside and outside the magnet, designed specifically for multi-sensory experimental paradigms. The frequency of whisker stimulation with this device could range from a few Hz to as much as 40 Hz, which seems to be the upper limit of naturalistic whisker stimulation [89].

In the same rat or across a group of rats, whisker stimulation induced multi-modal responses (of BOLD, CBF, and MUA) in the contralateral $S1_{BF}$ (Fig. 5). The induced response seemed to peak at stimulation frequencies between 8 and 12 Hz (Fig. 6) which is within the natural whisking frequency in rodents [89]. Earlier studies [90] have shown that CBF in the rat $S1_{BF}$ increases linearly with higher whisker movement frequencies. However future studies should investigate the neurophysiologic basis of the increased area of BOLD activation observed at the higher stimulation frequencies (Fig. 6). In summary, unilateral (and bilateral) whiskers stimulation with air puffs resulted in fMRI and neurophysiologic signal increases in the contralateral $S1_{BF}$ for consistent and reproducible studies, both in the same subject and across a group of subjects. While this device provides easy control of whisking

frequency, we are investigating more refined amplitude variations by controlling flow rates of compressed air.

Tactile: Forepaw stimulation—While ambulatory functions fulfilled by the rodent's forelimbs and hindlimbs may seem mundane compared to the perceptions of smell and whisking, somatosensory sensing by the limbs represent an important component of the multi-faceted environmental cues that a rodent must experience for survival. Upon stimulation of either limb, afferent signals arrive through the medial-lemniscal system at the contralateral ventral posterior lateral nucleus of the thalamus, prior to connecting with the limb-specific contralateral primary somatosensory cortex. Electrical stimulation of nerve fibers innervating the touch-sensitive limbs is the most widely used method of sensory stimulation of the rat, both in bench neurophysiologic [91–94] and fMRI [95–101] studies.

Forepaw stimulation in the rat is a very popular model in many fMRI laboratories [95–98] and can be easily applied identically inside and outside the magnet [98–101]. The pulse amplitude is typically in the range of a few mA and the pulse duration is usually a fraction of a ms. The electrodes are typically small enough to be placed subcutaneously in the forepaw's skin. It is easily applied and produces very well localized and strong electrical and hemodynamic cortical responses. During electrical forepaw stimulation, robust multi-modal activations in the contralateral $S1_{FL}$ were reproducibly observed in different sessions as well as across many subjects under α-chloralose anesthesia (Fig. 7,8). The peak $S1_{FL}$ response was near 1–3 Hz forepaw stimulation frequency [64,65] which is quite different from the $S1_{BF}$ response during whisker stimulation. This model has been widely used for biophysical/physiologic characterization of the BOLD image contrast [102–108], perhaps in part, because the averaged BOLD response localized in the contralateral $S1_{FL}$ is much larger than observed with other sensory modalities.

5.2 Challenges of *in vivo* NMR and bench experiments

We have described some experiences with anesthetized rat preparations in our laboratory. But the awake experiment still has desirable features. However the few fMRI studies that have reported on awake but restrained rats [109–111] do not demonstrate the same level of reproducibility in BOLD activations as anesthetized rats, perhaps in part, because the spontaneous BOLD oscillations can be as large as the induced BOLD responses [111] and furthermore even the BOLD responses can be quite variable [110]. We, and many others, hypothesize that “the anesthetic state may be thought of as a tool for limiting the repertoire of physiological responses of cortical neurons so that the most anesthesia-resistant properties can be readily identified” [112] and studied under controlled settings. “Such maps should not lead to false conclusion, however, that they define only the functions carried out in a given cortical region, or that the sensory properties are reflected in exactly the same physiological manner as in the awake [state]” [112]. Successful *in vivo* fMRI and neurophysiologic studies depends on maintenance of normal physiologic state and sustaining the appropriate depth of anesthesia. Whether the subject is awake or anesthetized, optimal shimming conditions for fMRI scans are always desirable. Below we discuss some insights into potential pitfalls and, where possible, how to avoid them.

Importance of physiological state—The well being of experimental animals, whether under anesthesia or awake, should be monitored and whenever possible controlled. Usually the overall physiologic state of the subject should be judged at three levels: central nervous system (e.g., by EEG, MUA), cardiovascular system (e.g., by blood pressure, heart rate), and respiratory system (e.g., by pCO_2, respiratory rate). In our studies, all three components are controlled and measured to assess the anesthetized state. To provide an effortless external ventilation for the respiratory control, we used neuromuscular blocking agents which do not

act on the central nervous system. Furthermore we monitor analgesic level frequently. Blood pressure provides a continuous indicator of anesthesia/analgesia depth as mildly noxious stimuli should not cause increases in the instantaneous pressure of more than ~10% [113]. Additional doses of anesthetic agent(s) must be applied if there are indications of discomfort.

Arterial blood samples drawn periodically to monitor pCO_2 and pH provide very important measures of systemic physiology. In the rat, the pCO_2 is in the range 35–40 mmHg under optimal steady-state conditions. High pCO_2 leads to a reduced pH and dilatation of vessel walls in an attempt to increase flow and thereby remove more of the potentially toxic acidic substances from tissue. This situation will also affect the baseline CBF level and therefore affect the BOLD response and its temporal dynamics. Low pCO_2 has the opposite effect. Both situations interfere with the tissue's ability to adjust flow in response to activity changes, thereby constituting a serious *caveat* to the interpretation of hyperemic responses.

In freely breathing animals, blood gas tension is a crucial factor in determining the physiological state of the anesthetized state. Excluding olfactory studies, we mechanically ventilated through a tracheotomy and controlled both the rate and volume of breathing. Although buffering mechanisms in the blood exist to keep the pH within a narrow optimal range (~7.4), they are not able to do so indefinitely in a situation where breathing parameters are not suitably adjusted and pCO_2 levels span out of optimal range. The core temperature of the animal also influences the acid-base balance of the blood, and must be maintained stable (~37 °C) despite the cool temperatures in the imaging bore (~18 °C). In the case of a drop in pH of metabolic origin, such as acidosis caused by the anesthetic urethane [114], periodic intravenous injections of sodium bicarbonate can be used to stabilize the animal and obtain reliable hyperemic responses.

Effect of anesthesia—Anesthetics have been valuable in neuroscience to understand the effects of afferent inputs on localized regions of the brain [115–117] because most peripheral stimuli (i.e., auditory, visual, olfactory, limbs, whiskers) still reach the brain with anesthesia. Most tactile stimuli still arrive at the cortex because peripheral nerve conduction and transmission at the neuromuscular junction seem to be negligibly affected by anesthetics. Non-tactile signal transduction, for the most part, is not limited by the neuromuscular junction and therefore these stimuli expeditiously reach the brain because of more direct pathways into the brain.

Most anesthetics act on different levels of neuronal signaling by depressed axonal conductance of action potentials, modified dendritic and somatic integration, reduced presynaptic neurotransmitter release, and/or altered postsynaptic receptors. The $GABA_A$ receptor is commonly considered to be an important molecular target since it seems to be ubiquitously affected by most anesthetics. A notable exception is urethane, the effect of which appears to be mediated by the enhanced conductance of a specific potassium-channel subtype [118]. Anesthetics, inhaled or injected, reduce brain energy consumption rather uniformly across regions and cortical energy decline is typically monotonic with anesthetic depth [119]. Consistent with this observation, anesthetics also depress firing rates and impede slow field oscillations of excitatory pyramidal cortical neurons [120].

Use of anesthesia during rodent fMRI and neurophysiology is needed to ensure immobilization and comfort during long experiments under physically constrained circumstances. Many reports on the “confounding effects” of anesthesia exist in the literature [121,122], pointing to the inherent limitation of studying neural systems under abnormal (i.e., non-awake) conditions [123]. Our belief is that although the full complexity of awake brain responses to sensory stimuli clearly cannot be reached under anesthesia,

important insights into general functional properties a given sensory system can be made [29]. Combined with the detailed knowledge of morphological, functional, vascular, and neuronal properties of rat brain tissue, results obtained in the anesthetized preparation can be extrapolated and generalized towards the awake brain. The common response features obtained under multiple different anesthetics to the same stimulation, in our laboratory and others, offers indirect support to the generality of the results.

Magnetic susceptibility effects and "shimming"—Despite the high NMR sensitivity at 11.7T, there are some challenges. Magnetic susceptibility is a property of matter indicating its propensity to become (para)magnetic upon introduction into a magnetic field. It is analogous to polarization of insulators in an electric field. The BOLD effect is a consequence of a dynamic process of "microscopic" magnetic susceptibility changes occurring as the concentration of oxygen-rich blood varies during a functional challenge [5,6]. However interfaces between substances with different magnetic susceptibilities lead to "macroscopic" signal loss near the boundary between media. In the rodent, regions with such interfaces leading to signal degeneration include the inferior temporal lobes adjacent to air-filled ear canals, the caudal occipital lobes in which the tissues separating the cortex from the cerebellum appear in the imaging plane, and the olfactory bulb embedded in bony and cartilaginous tissue surrounded by mucous membranes.

"Shimming" is a process of applying small corrective magnetic field gradients onto the main static magnetic field in order to optimize field homogeneity in and around the sample. It is a procedure to reduce structurally imposed signal loss, mainly at the media interfaces, by correcting for gross susceptibility-induced magnetic field inhomogeneities. Since the correction of "macroscopic" magnetic field inhomogeneities becomes increasingly important at higher fields, some automatic routines have been developed [45,124–126].

For high sensitivity fMRI studies it is crucial that the surface coil be as close to the brain as possible. Therefore it seems obvious that the removal of the scalp (skin, galea aponeurotica) and periosteum should improve the signal intensity from the brain since the whole brain moves closer to the coil. However this approach will also move the air-tissue (bone) interface closer to the tissue of interest (brain), which in turn may lead to field inhomogeneities beyond the capabilities of the shim gradients. We avoid the scalp removal procedure whenever possible, focusing instead on careful positioning of the animal and shimming.

There is a special shimming problem in the case of olfactory bulb imaging. Since the nasal cavity is very close to the olfactory bulb, changes in the level of mucous secretion will affect the local susceptibility, and thereby the shimming. A stable physiological condition of the nasal epithelium during odor delivery experiments is required not only to prevent these adverse magnetic inhomogeneity effects on the measured signal, but also to ensure the odorant molecules' access to the epithelial odorant receptors. A common choice of anesthetic in rodent fMRI studies, α-chloralose, causes thick mucoid oral-nasal discharge [127]. For odor stimulations we used urethane – a long lasting anesthetic with excellent analgesic properties – the general use of which though must be discouraged for survival studies because of its carcinogenic and mutagenic effects. In addition to the choice of anesthetic, we carefully controlled the temperature of the incoming air to the animal by pre-heating it to 28–30 °C, close to the core temperature maintained at ~37 °C, to prevent mucous accumulation due to the low ambient temperature (~18 °C) within the imaging bore.

5.3 Future directions

In recent years, careful refinement of the BOLD effect to reveal its physiologic basis [15–23,29] for future diagnostic use has been quite encouraging [12–14]. However it should be

acknowledged that these studies have primarily focused on neuronal functions where the role of their glial counterpart has been largely neglected [128,129]. Therefore another potential direction that animal models, such as the ones described here, may help with is the information about the glial activities that accompany neuronal and/or BOLD signal changes. But this endeavor would require development of glial-specific NMR and non-NMR methods to complement the plethora of neuron-specific measurements that currently exist and are routinely used in many laboratories.

Localized NMR data collection, for MRI as well as for MRS, is based on imposing linear field gradients which are rapidly alternated at a rate of several hundred times per second. The gradients are generated by currents passing through coils of various shape and orientation around the sample. The mechanical Lorenz force acting upon the gradient coils, particularly during EPI scans for fMRI, generates waves which are audible as loud “clicks” or “blibs” in and around the scanner. Since this is a continuous noise source during our studies, its affect can be partly negated. We are currently investigating possibilities of applying noise-cancellation techniques for future studies. However studying the auditory system is a considerable challenge with fMRI because of susceptibility-induced signal losses near the ear canals, in particular in the temporal auditory cortices. Nevertheless some methods are being developed [123] which may alleviate the shimming troubles in such brain locations.

The developments presented here, and more plans underway, are readily applicable to studying effects of different tactile (i.e., forepaw, whisker) and non-tactile (i.e., olfactory, visual) modalities simultaneously. Meredith and Stein [130,131] defined two classes of multi-sensory interactions within the receptive fields of cortical neurons: response enhancement and response depression. Though it appears to be a general mechanism in the central nervous system, one region in which such multi-sensory convergence and synthesis takes place *en masse* is the SC, situated in the dorsal mid-brain, caudal to the thalamus. In the cat SC, Meredith and Stein [130] showed that a conservative estimate to the lower limit of the proportion of cells exhibiting multi-sensory interactions in the intermediate and deep laminae of the SC is 50%, the majority of which project efferent fibers to sensorimotor areas of the brain stem and spinal cord. These findings are consistent with the hypothesized role of the SC in the control of eye, head, and body movements underlying rapid orientation towards external objects. The results from our visual stimulation paradigm illustrate reproducible BOLD responses in the superficial laminae of the SC. Therefore we are now in a position to begin fMRI and neurophysiologic studies of sensory integration with tactile and/or non-tactile sensory stimuli.

Acknowledgments

We thank Dr. Fuqiang Xu (Wuhan Institute of Physics and Mathematics, Wuhan, China) for help during preliminary stages of olfactory bulb imaging. We appreciate valuable inputs from Dr. Lawrence B. Cohen (Yale University) and his laboratory members (i.e., Drs. Ryota Homma and Efstratios Kosmidis) regarding the design of the olfactometer. We are grateful to Alyssa Siefert (a summer internship student from Carnegie Mellon University) and Scott McIntyre (an MRRC engineer) for the initial design of the visual stimulation device. We are also extremely appreciative of other MRRC/QNMR engineers and staff (i.e., Terry Nixon, Peter Brown, Mark Abildgaard, Bei Wang) for assistance in other parts of our experimental setup. This work was supported by personal grants to CJB (Dagmar Marshall's Fond, Frimodts Fond and Oticon Fonden), the Hungarian Research Foundation grant to PH (OTKA-T34122), and National Institutes of Health grants to FH (R01 MH-067528, R01 DC-003710, P30 NS-52519).

7. References

1. Raichle, ME. Handbook of physiology - The nervous system V. Springer-Verlag; New York, USA: 1988. Circulatory and metabolic correlates of brain function in normal humans; p. 633-674.

2. Raichle ME. Behind the scenes of functional brain imaging: A historical and physiological perspective. Proc Natl Acad Sci USA. 1998; 95:765–772. [PubMed: 9448239]

3. Shulman RG, Blamire AM, Rothman DL, McCarthy G. Nuclear magnetic resonance imaging and spectroscopy of human brain function. Proc Natl Acad Sci USA. 1993; 90:3127–3133. [PubMed: 8475050]

4. Shulman RG, Rothman DL, Behar KL, Hyder F. Energetic basis of brain activity: Implications for neuroimaging. Trends Neurosci. 2004; 27:489–495. [PubMed: 15271497]

5. Ogawa S, Lee TM, Nayak AS, Glynn P. Oxygenation-sensitive contrast in magnetic resonance image on rodent brain at high magnetic fields. Magn Reson Med. 1990; 14:68–78. [PubMed: 2161986]

6. Ogawa S, Menon RS, Tank DW, Kim SG, Merkle H, Ellermann JM, Ugurbil K. Functional brain mapping by blood oxygenation level-dependent contrast magnetic resonance imaging. Biophys J. 1993; 64:803–812. [PubMed: 8386018]

7. Bandettini PA, Wong EC, Hinks RS, Tikofsky RS, Hyde JS. Time course EPI of human brain function during task activation. Magn Reson Med. 1992; 25:390–397. [PubMed: 1614324]

8. Blamire AM, Ogawa S, Ugurbil K, Rothman D, Mccarthy G, Ellermann JM, Hyder F, Rattner Z, Shulman RG. Dynamic mapping of the human visual cortex by high-speed magnetic resonance imaging. Proc Natl Acad Sci USA. 1992; 89:11069–11073. [PubMed: 1438317]

9. Kwong KW, Belliveau JW, Chesler DA, Goldberg IE, Weiskoff RM, Poncelet BP, Kennedy DN, Hoppel BE, Cohen MS, Turner R, Cheng HM, Brady TJ, Rosen BR. Dynamic magnetic resonance imaging of human brain activity during primary sensory stimulation. Proc Natl Acad Sci USA. 1992; 89:5675–5679. [PubMed: 1608978]

10. Ogawa S, Tank DW, Menon R, Ellermann JM, Kim SG, Merkle H, Ugurbil K. Intrinsic signal changes accompanying sensory stimulation: Functional brain mapping with magnetic resonance imaging. Proc Natl Acad Sci USA. 1992; 89:5951–5955. [PubMed: 1631079]

11. Posner MI, Raichle ME. The neuroimaging of human brain function. Proc Natl Acad Sci USA. 1998; 95:763–764. [PubMed: 9448238]

12. Logothetis NK. The neural basis of the blood-oxygen-level-dependent functional magnetic resonance imaging signal. Philos Trans R Soc Lond B Biol Sci. 2002; 357:1003–1037. [PubMed: 12217171]

13. Lauritzen M. Relationship of spikes, synaptic activity, and local changes of cerebral blood flow. J Cereb Blood Flow Metab. 2001; 21:1367–1383. [PubMed: 11740198]

14. Hyder F. Neuroimaging with calibrated fMRI. Stroke. 2004; 35(Suppl 1):2635–2641. [PubMed: 15388903]

15. Logothetis NK, Pauls J, Augath M, Trinath T, Oeltermann A. Neurophysiological investigation of the basis of the fMRI signal. Nature. 2001; 412:150–157. [PubMed: 11449264]

16. Smith AJ, Blumenfeld H, Behar KL, Rothman DL, Shulman RG, Hyder F. Cerebral energetics and spiking frequency: The neurophysiological basis of fMRI. Proc Natl Acad Sci USA. 2002; 99:10765–10770. [PubMed: 12134056]

17. Kim DS, Ronen I, Olman C, Kim SG, Ugurbil K, Toth LJ. Spatial relationship between neuronal activity and BOLD functional MRI. NeuroImage. 2004; 21:876–885. [PubMed: 15006654]

18. Arthurs OJ, Williams EJ, Carpenter TA, Pickard JD, Boniface SJ. Linear coupling between functional magnetic resonance imaging and evoked potential amplitude in human somatosensory cortex. Neuroscience. 2000; 101:803–806. [PubMed: 11113329]

19. Rees G, Friston K, Koch C. A direct quantitative relationship between the functional properties of human and macaque V5. Nat Neurosci. 2000; 3:716–723. [PubMed: 10862705]

20. Niessing J, Ebisch B, Schmidt KE, Niessing M, Singer W, Galuske RA. Hemodynamic signals correlate tightly with synchronized gamma oscillations. Science. 2005; 309:948–951. [PubMed: 16081740]

21. Kida I, Smith AJ, Blumenfeld H, Behar KL, Hyder F. Lamotrigine suppresses neurophysiological responses to somatosensory stimulation in the rodent. NeuroImage. 2006; 29:216–224. [PubMed: 16112588]

22. Gsell W, Burke M, Wiedermann D, Bonvento G, Silva AC, Dauphin F, Buhrle C, Hoehn M, Schwindt W. Differential effects of NMDA and AMPA glutamate receptors on functional

magnetic resonance imaging signals and evoked neuronal activity during forepaw stimulation of the rat. J Neurosci. 2006; 26:8409–8416. [PubMed: 16914666]

23. Burke M, Buhrle C. BOLD response during uncoupling of neuronal activity and CBF. NeuroImage. 2006; 32:1–8. [PubMed: 16677832]
24. Hyder F, Behar KL, Martin MA, Blamire AM, Shulman RG. Dynamic magnetic resonance imaging of the rat brain during forepaw stimulation. J Cereb Blood Flow Metab. 1994; 14:649–655. [PubMed: 8014212]
25. Yang X, Hyder F, Shulman RG. Single-whisker activation observed in rat cortex by functional magnetic resonance imaging. Proc Natl Acad Sci USA. 1996; 93:475–478. [PubMed: 8552664]
26. Xu F, Kida I, Hyder F, Shulman RG. Assessment and discrimination of odor stimuli in rat olfactory bulb by dynamic fMRI. Proc Natl Acad Sci USA. 2000; 97:10601–10606. [PubMed: 10973488]
27. Ugurbil K, Adriany G, Andersen P, Chen W, Garwood M, Gruetter R, Henry PG, Kim SG, Lieu H, Tkac I, Vaughan T, Van De Moortele PF, Yacoub E, Zhu XH. Ultrahigh field magnetic resonance imaging and spectroscopy. Magn Reson Imaging. 2003; 21:1263–1281. [PubMed: 14725934]
28. Schafer JR, Kida I, Rothman DL, Xu F, Hyder F. Reproducibility of odor maps by fMRI in rodents. NeuroImage. 2006; 31:1238–1246. [PubMed: 16632382]
29. Maandag NJG, Coman D, Sanganahalli BG, Herman P, Blumenfeld H, Smith AJ, Shulman RG, Hyder F. Energetics of neuronal signaling and fMRI activity. Proc Natl Acad Sci USA. 2007 in press.
30. Kida I, Maciejewski PK, Hyder F. Dynamic imaging of perfusion and oxygenation by fMRI. J Cereb Blood Flow Metab. 2004; 24:1369–1281. [PubMed: 15625411]
31. Kida I, Rothman DL, Hyder F. Dynamics of changes in blood flow, volume, and oxygenation: Implications for dynamic fMRI calibration. J Cereb Blood Flow Metab. 2007; 27:690–696. [PubMed: 17033688]
32. Shepherd, GM. The synaptic organization of the brain. Oxford University Press; New York: 2004.
33. Wallace MT, Meredith MA, Stein BE. Converging influences from visual, auditory, and somatosensory cortices onto output neurons of the superior colliculus. J Neurophysiol. 1993; 69:1797–1809. [PubMed: 8350124]
34. Wallace MT, Meredith MA, Stein BE. Multisensory integration in the superior colliculus of the alert cat. J Neurophysiol. 1998; 80:1006–1010. [PubMed: 9705489]
35. Kauer JS. Response patterns of amphibian olfactory bulb neurones to odour stimulation. J Physiol. 1974; 243:695–715. [PubMed: 4548720]
36. Zochowski M, Cohen LB, Fuhrmann G, Kleinfeld D. Distributed and partially separate pools of neurons are correlated with two different components of the gill-withdrawal reflex in Aplysia. J Neurosci. 2000; 20:8485–8492. [PubMed: 11069956]
37. Van Camp N, Verhoye M, De Zeeuw CI, Van der Linden A. Light stimulus frequency dependence of activity in the rat visual system as studied with high-resolution BOLD fMRI. J Neurophysiol. 2006; 95:3164–3170. [PubMed: 16394078]
38. Schulte ML, Pawela CP, Cho YR, Li R, Hudetz AG, Hyde JS. Detecting responses to single light flashes in the rodent brain using laser Doppler and fMRI at 9.4T. Proc Int Soc Magn Reson Med. 2007; 15:3214.
39. Rooney BJ, Cooper RM. Effects of square-wave gratings and diffuse light on metabolic activity in the rat visual system. Brain Res. 1988; 439:311–321. [PubMed: 3359191]
40. Prusky GT, West PW, Douglas RM. Reduced visual acuity impairs place but not cued learning in the Morris water task. Behav Brain Res. 2002; 116:135–140. [PubMed: 11080544]
41. Lund RD, Lund JS, Wise RP. The organization of the retinal projection to the dorsal lateral geniculate nucleus in pigmented and albino rats. J Comp Neurol. 1974; 158:383–403. [PubMed: 4448860]
42. Drager UC, Olsen JF. Origins of crossed and uncrossed retinal projections in pigmented and albino mice. J Comp Neurol. 1980; 191:383–412. [PubMed: 7410600]
43. Abel PL, Olavarria JF. The callosal pattern in striate cortex is more patchy in monocularly enucleated albino than pigmented rats. Neurosci Lett. 1996; 204:169–172. [PubMed: 8938257]

44. Nersesyan H, Hyder F, Rothman DL, Blumenfeld H. Dynamic fMRI and EEG recordings during spike-wave seizures and generalized tonic-clonic seizures in WAG/Rij rats. J Cereb Blood Flow Metab. 2004; 24:589–599. [PubMed: 15181366]
45. Gruetter R. Automatic, localized in vivo adjustment of all first- and second-order shim coils. Magn Reson Med. 1993; 29:804–811. [PubMed: 8350724]
46. Hennig J, Nauerth A, Friedburg H. RARE imaging: a fast imaging method for clinical MR. Magn Reson Med. 1986; 3:823–833. [PubMed: 3821461]
47. Frahm J, Haase A, Matthaei D. Rapid three-dimensional MR imaging using the FLASH technique. J Comput Assist Tomogr. 1986; 10:363–368. [PubMed: 3950172]
48. Mansfield P. Multi-planar iImage formation using NMR spin echoes. J Phys C. 1977; 10:L55–L58.
49. Hyder F, Rothman DL, Blamire AM. Image reconstruction of sequentially sampled echo-planar data. Magn Reson Imaging. 1995; 13:97–103. [PubMed: 7898286]
50. Nersesyan H, Herman P, Erdogan E, Hyder F, Blumenfeld H. Relative changes in cerebral blood flow and neuronal activity in local microdomains during generalized seizures. J Cereb Blood Flow Metab. 2004; 24:1057–1068. [PubMed: 15356426]
51. Trubel HKF, Sacolick LI, Hyder F. Regional temperature changes in the brain during somatosensory stimulation. J Cereb Blood Flow Metab. 2006; 26:68–78. [PubMed: 15959461]
52. Schridde U, Khubchandani M, Motelow JE, Sanganahalli BG, Hyder F, Blumenfeld H. Negative BOLD with large increases in neuronal activity. Cereb Cortex. 2007 in press.
53. Paxinos, G.; Watson, C. The Rat Brain in Stereotaxic Coordinates. Academic Press; New York, NY: 1997.
54. Yang X, Renken R, Hyder F, Siddeek M, Greer CA, Shepherd GM, Shulman RG. Dynamic mapping at the laminar level of odor-elicited responses in rat olfactory bulb by functional MRI. Proc Natl Acad Sci USA. 1998; 95:7715–7720. [PubMed: 9636216]
55. Xu F, Liu N, Kida I, Rothman DL, Hyder F, Shepherd GM. Odor maps of aldehydes and esters revealed by fMRI in the glomerular layer of the mouse olfactory bulb. Proc Natl Acad Sci USA. 2003; 100:11029–11034. [PubMed: 12963819]
56. Schafer JR, Kida I, Rothman DL, Hyder F, Xu F. Adaptation in the rodent olfactory bulb measured with fMRI. Magn Reson Med. 2005; 54:443–448. [PubMed: 16032685]
57. Beuerman RW. Slow potentials of the turtle olfactory bulb in response to odor stimulation of the nose. Brain Res. 1975; 97:61–78. [PubMed: 1175040]
58. Lam YW, Cohen LB, Wachowiak M, Zochowski MR. Odors elicit three different oscillations in the turtle olfactory bulb. J Neurosci. 2000; 20:749–762. [PubMed: 10632604]
59. Woolsey TA. Some anatomical bases of cortical somatotopic organization. Brain Behav Evol. 1978; 15:325–371. [PubMed: 737526]
60. Simons DJ. Multi-whisker stimulation and its effects on vibrissa units in rat SmI barrel cortex. Brain Res. 1983; 276:178–182. [PubMed: 6626997]
61. Welker E. Developmental plasticity: to preserve the individual or to create a new species? Novartis Found Symp. 2000; 228:227–235. [PubMed: 10929325]
62. Yang X, Hyder F, Shulman RG. Functional MRI BOLD signal coincides with electrical activity in rat whisker barrel. Magn Reson Med. 1997; 38:874–877. [PubMed: 9402186]
63. Keilholz SD, Silva AC, Raman M, Merkle H, Koretsky AP. Functional MRI of the rodent somatosensory pathway using multislice echo planar imaging. Magn Reson Med. 2004; 52:89–99. [PubMed: 15236371]
64. Brinker G, Bock C, Busch E, Krep H, Hossmann KA, Hoehn-Berlage M. Simultaneous recording of evoked potentials and T2*-weighted MR images during somatosensory stimulation of rat. Magn Reson Med. 1999; 41:469–473. [PubMed: 10204868]
65. Van Camp N, Verhoye M, Van der Linden A. Stimulation of the rat somatosensory cortex at different frequencies and pulse widths. NMR Biomed. 2006; 19:10–17. [PubMed: 16408324]
66. Shepherd, GM.; Chen, WR.; Greer, CA. Olfactory bulb. In: Shepherd, GM., editor. The synaptic organization of the brain. Oxford University Press; New York: 2004. p. 165-216.
67. Johnson BA, Leon M. Odorant molecular length: one aspect of the olfactory code. J Comp Neurol. 2000; 426:330–338. [PubMed: 10982472]

68. Bozza T, McGann JP, Mombaerts P, Wachowiak M. In vivo imaging of neuronal activity by targeted expression of a genetically encoded probe in the mouse. Neuron. 2004; 42:9–21. [PubMed: 15066261]
69. Fried HU, Fuss SH, Korsching SI. Selective imaging of presynaptic activity in the mouse olfactory bulb shows concentration and structure dependence of odor responses in identified glomeruli. Proc Natl Acad Sci USA. 2002; 99:3222–3227. [PubMed: 11854464]
70. Meister M, Bonheoffer T. Tuning and topography in an odor map on the rat olfactory bulb. J. Neurosci. 2001; 21:1351–1360. [PubMed: 11160406]
71. Mori K, Takahashi YK, Igarashi KM, Yamaguchi M. Maps of odorant molecular features in the Mammalian olfactory bulb. Physiol Rev. 2006; 86:409–433. [PubMed: 16601265]
72. Xu F, Schaefer M, Kida I, Schafer JR, Liu N, Rothman DL, Hyder F, Restrepo D, Shepherd GM. Simultaneous activation of mouse main and accessory olfactory bulbs by odors or pheromones. J Comp Neurol. 2005; 489:491–500. [PubMed: 16025460]
73. Martin C, Grenier D, Thevenet M, Vigouroux M, Bertrand B, Janier M, Ravel N, Litaudon P. fMRI visualization of transient activations in the rat olfactory bulb using short odor stimulations. NeuroImage. 2007; 36:1288–1293. [PubMed: 17512755]
74. Kida I, Xu F, Shulman RG, Hyder F. Mapping at glomerular resolution: fMRI of rat olfactory bulb. Magn. Reson. Med. 2002; 48:570–576. [PubMed: 12210928]
75. Liu N, Xu F, Marenco L, Hyder F, Miller P, Shepherd GM. Informatics approaches to functional MRI odor mapping of the rodent olfactory bulb: OdorMapBuilder and OdorMapDB. Neuroinformatics. 2004; 2:3–18. [PubMed: 15067166]
76. Jakob PM, Griswold MA, Edelman RR, Manning WJ, Sodickson DK. Accelerated cardiac imaging using the SMASH technique. J Cardiovasc Magn Reson. 1999; 1:153–157. [PubMed: 11550348]
77. Pruessmann KP, Weiger M, Scheidegger MB, Boesiger P. SENSE: Sensitivity encoding for fast MRI. Magn Reson Med. 1999; 42:952–962. [PubMed: 10542355]
78. Holscher C, Schnee A, Dahmen H, Setia L, Mallot HA. Rats are able to navigate in virtual environments. J Exp Biol. 2005; 208:561–569. [PubMed: 15671344]
79. Sterling, P.; Demb, JB. Retina. In: Shepherd, GM., editor. The synaptic organization of the brain. Oxford University Press; New York: 2004. p. 217-269.
80. Jacobs GH, Fenwick JA, Williams GA. Cone-based vision of rats for ultraviolet and visible lights. J Exp Biol. 2001; 204:2439–2446. [PubMed: 11511659]
81. Adams AD, Forrester JM. The projection of the rat's visual field on the cerebral cortex. Q J Exp Physiol Cogn Med Sci. 1968; 53:327–336. [PubMed: 5188317]
82. Gias C, Hewson-Stoate N, Jones M, Johnston D, Mayhew JE, Coffey PJ. Retinotopy within rat primary visual cortex using optical imaging. NeuroImage. 2005; 24:200–206. [PubMed: 15588611]
83. Lund RD. Anatomic studies on the superior colliculus. Invest Ophthalmol. 1972; 11:434–441. [PubMed: 4624289]
84. Girman SV, Sauve Y, Lund RD. Receptive field properties of single neurons in rat primary visual cortex. J Neurophysiol. 1999; 82:301–311. [PubMed: 10400959]
85. Ohki K, Chung S, Ch'ng YH, Kara P, Reid RC. Functional imaging with cellular resolution reveals precise micro-architecture in visual cortex. Nature. 2005; 433:597–603. [PubMed: 15660108]
86. Woolsey TA, Van der Loos H. The structural organization of layer IV in the somatosensory region (SI) of mouse cerebral cortex. The description of a cortical field composed of discrete cytoarchitectonic units. Brain Res. 1970; 17:205–242. [PubMed: 4904874]
87. Welker C, Woolsey TA. Structure of layer IV in the somatosensory neocortex of the rat: description and comparison with the mouse. J Comp Neurol. 1974; 158:437–453. [PubMed: 4141363]
88. Lu H, Mazaheri Y, Zhang R, Jesmanowicz A, Hyde JS. Multishot partial-k-space EPI for high-resolution fMRI demonstrated in a rat whisker barrel stimulation model at 3T. Magn Reson Med. 2003; 50:1215–1222. [PubMed: 14648569]
89. Simons DJ. Response properties of vibrissa units in rat SI somatosensory neocortex. J Neurophys. 1978; 41:798–820.

90. Gerrits RJ, Stein EA, Greene AS. Blood flow increases linearly in rat somatosensory cortex with increased whisker movement frequency. Brain Res. 1998; 783:151–157. [PubMed: 9479064]

91. Ances BM, Zarahn E, Greenberg JH, Detre JA. Coupling of neural activation to blood flow in the somatosensory cortex of rats is time-intensity separable, but not linear. J Cereb Blood Flow Metab. 2000; 20:921–930. [PubMed: 10894175]

92. Blood AJ, Pouratian N, Toga AW. Temporally staggered forelimb stimulation modulates barrel cortex optical intrinsic signal responses to whisker stimulation. J Neurophysiol. 2002; 88:422–437. [PubMed: 12091565]

93. Buerk DG, Ances BM, Greenberg JH, Detre JA. Temporal dynamics of brain tissue nitric oxide during functional forepaw stimulation in rats. NeuroImage. 2003; 18:1–9. [PubMed: 12507439]

94. Sheth SA, Nemoto M, Guiou M, Walker M, Pouratian N, Toga AW. Linear and nonlinear relationships between neuronal activity, oxygen metabolism, and hemodynamic responses. Neuron. 2004; 42:347–355. [PubMed: 15091348]

95. Xu S, Yang J, Li CQ, Zhu W, Shen J. Metabolic alterations in focally activated primary somatosensory cortex of alpha-chloralose-anesthetized rats measured by 1H MRS at 11.7 T. NeuroImage. 2005; 28:401–409. [PubMed: 16182571]

96. Morton DW, Keogh B, Lim K, Maravilla KR. Functional brain imaging using a long intravenous half-life gadolinium-based contrast agent. Am J Neuroradiol. 2006; 27:1467–1471. [PubMed: 16908560]

97. Lowe AS, Beech JS, Williams SC. Small animal, whole brain fMRI: Innocuous and nociceptive forepaw stimulation. NeuroImage. 2007; 35:719–728. [PubMed: 17300960]

98. Ogawa S, Lee TM, Stepnoski R, Chen W, Zhu XH, Ugurbil K. An approach to probe some neural systems interaction by functional MRI at neural time scale down to milliseconds. Proc Natl Acad Sci USA. 2000; 97:11026–11031. [PubMed: 11005873]

99. Kuo CC, Chen JH, Tsai CY, Liang KC, Yen CT. BOLD signals correlate with ensemble unit activities in rat's somatosensory cortex. Chin J Physiol. 2005; 48:200–209. [PubMed: 16548422]

100. Stefanovic B, Schwindt W, Hoehn M, Silva AC. Functional uncoupling of hemodynamic from neuronal response by inhibition of neuronal nitric oxide synthase. J Cereb Blood Flow Metab. 2007; 27:741–754. [PubMed: 16883353]

101. Huttunen JK, Grohn O, Penttonen M. Coupling between simultaneously recorded BOLD response and neuronal activity in the rat somatosensory cortex. NeuroImage. 2007 in press.

102. Lee SP, Silva AC, Ugurbil K, Kim SG. Diffusion-weighted spin-echo fMRI at 9.4 T: microvascular/tissue contribution to BOLD signal changes. Magn Reson Med. 1999; 42:919–928. [PubMed: 10542351]

103. Silva AC, Lee SP, Yang G, Iadecola C, Kim SG. Simultaneous blood oxygenation level-dependent and cerebral blood flow functional magnetic resonance imaging during forepaw stimulation in the rat. J Cereb Blood Flow Metab. 1999; 19:871–879. [PubMed: 10458594]

104. Mandeville JB, Marota JJ, Ayata C, Moskowitz MA, Weisskoff RM, Rosen BR. MRI measurement of the temporal evolution of relative CMRO2 during rat forepaw stimulation. Magn Reson Med. 1999; 42:944–951. [PubMed: 10542354]

105. Kennan RP, Jacob RJ, Sherwin RS, Gore JC. Effects of hypoglycemia on functional magnetic resonance imaging response to median nerve stimulation in the rat brain. J Cereb Blood Flow Metab. 2000; 20:1352–1359. [PubMed: 10994857]

106. Kida I, Hyder F, Behar KL. Inhibition of voltage-dependent sodium channels suppresses the functional magnetic resonance imaging response to forepaw somatosensory activation in the rodent. J Cereb Blood Flow Metab. 2001; 21:585–591. [PubMed: 11333369]

107. Hyder F, Kida I, Behar KL, Kennan RP, Maciejewski PK, Rothman DL. Quantitative functional imaging of the brain: Towards mapping neuronal activity by BOLD fMRI. NMR Biomed. 2001; 14:413–431. [PubMed: 11746934]

108. Liu ZM, Schmidt KF, Sicard KM, Duong TQ. Imaging oxygen consumption in forepaw somatosensory stimulation in rats under isoflurane anesthesia. Magn Reson Med. 2004; 52:277–285. [PubMed: 15282809]

109. Lahti KM, Ferris CF, Li F, Sotak CH, King JA. Comparison of evoked cortical activity in conscious and propofol-anesthetized rats using functional MRI. Magn Reson Med. 1999; 41:412–426. [PubMed: 10080292]

110. Peeters RR, Tindemans I, De Schutter E, Van der Linden A. Comparing BOLD fMRI signal changes in the awake and anesthetized rat during electrical forepaw stimulation. Magn Reson Imaging. 2001; 19:821–826. [PubMed: 11551722]

111. Sachdev RN, Champney GC, Lee H, Price RR, Pickens DR 3rd, Morgan VL, Stefansic JD, Melzer P, Ebner FF. Experimental model for functional magnetic resonance imaging of somatic sensory cortex in the unanesthetized rat. NeuroImage. 2003; 19:742–750. [PubMed: 12880803]

112. Chapin JK, Lin CS. Mapping the body representation in the SI cortex of anesthetized and awake rats. J Comp Neurol. 1984; 229:199–213. [PubMed: 6438190]

113. Kohn, DF.; Wixson, SK.; White, WJ.; Benson, GJ. Anesthesia and Analgesia in Laboratory Animals. Academic Press; New York, USA: 1997.

114. Alfaro V, Palacios L. Components of the blood acid-base disturbance that accompanies urethane anaesthesia in rats during normothermia and hypothermia. Clin Exp Pharmacol Physiol. 1997; 24:498–502. [PubMed: 9248667]

115. Adrian ED. Afferent discharges to the cerebral cortex from peripheral sense organs. J Physiol. 1941; 100:159–191. [PubMed: 16991516]

116. Mountcastle VB. Modality and topographic properties of single neurons of cat's somatic sensory cortex. J Neurophysiol. 1957; 20:408–434. [PubMed: 13439410]

117. John ER. High nervous functions: Brain functions and learning. Annu Rev Physiol. 1961; 23:451–484. [PubMed: 13790206]

118. Sceniak MP, Maciver MB. Cellular actions of urethane on rat visual cortical neurons in vitro. J Neurophysiol. 2006; 95:3865–3874. [PubMed: 16510775]

119. Siesjo, BK. Brain Energy Metabolism. Wiley and Sons; New York, USA: 1978.

120. Antkowiak B. How do general anaesthetics work? Naturwissenschaften. 2001; 88:201–213. [PubMed: 11482433]

121. Bonvento G, Charbonne R, Correze JL, Borredon J, Seylaz J, Lacombe P. Is alpha-chloralose plus halothane induction a suitable anesthetic regimen for cerebrovascular research? Brain Res. 1994; 665:213–221. [PubMed: 7895056]

122. Austin VC, Blamire AM, Allers KA, Sharp T, Styles P, Matthews PM, Sibson NR. Confounding effects of anesthesia on functional activation in rodent brain: A study of halothane and alpha-chloralose anesthesia. NeuroImage. 2005; 24:92–100. [PubMed: 15588600]

123. Curtis JC, Kleinfeld D. Seeing what the mouse sees with its vibrissae: A matter of behavioral state. Neuron. 2006; 50:524–526. [PubMed: 16701202]

124. Shen J, Rothman DL, Hetherington HP, Pan JW. Linear projection method for automatic slice shimming. Magn Reson Med. 1999; 42:1082–1088. [PubMed: 10571929]

125. Miyasaka N, Takahashi K, Hetherington HP. Fully automated shim mapping method for spectroscopic imaging of the mouse brain at 9.4 T. Magn Reson Med. 2006; 55:198–202. [PubMed: 16270332]

126. Koch KM, Sacolick LI, Nixon TW, McIntyre S, Rothman DL, de Graaf RA. Dynamically shimmed multivoxel 1H magnetic resonance spectroscopy and multislice magnetic resonance spectroscopic imaging of the human brain. Magn Reson Med. 2007; 57:587–591. [PubMed: 17326186]

127. Wixson, SK.; Smiler, KL. Anesthesia and analgesia in rodents. In: Kohn, DF.; Wixson, SK.; White, WJ.; Benson, GJ., editors. Anesthesia and Analgesia in Laboratory Animals. Academic Press; New York, USA: 1997. p. 165-200.

128. Hyder F, Patel AB, Gjedde A, Rothman DL, Behar KL, Shulman RG. Neuronal-glial glucose oxidation and glutamatergic-GABAergic function. J Cereb Blood Flow Metab. 2006; 26:865–877. [PubMed: 16407855]

129. Iadecola C, Nedergaard M. Glial regulation of the cerebral microvasculature. Nat Neurosci. 2007; 10:1369–1376. [PubMed: 17965657]

130. Meredith MA, Stein BE. Visual, auditory, and somatosensory convergence on cells in superior colliculus results in multisensory integration. J Neurophysiol. 1986; 56:640–662. [PubMed: 3537225]

131. Meredith MA, Stein BE. Spatial determinants of multisensory integration in cat superior colliculus neurons. J Neurophysiol. 1996; 75:1843–1857. [PubMed: 8734584]

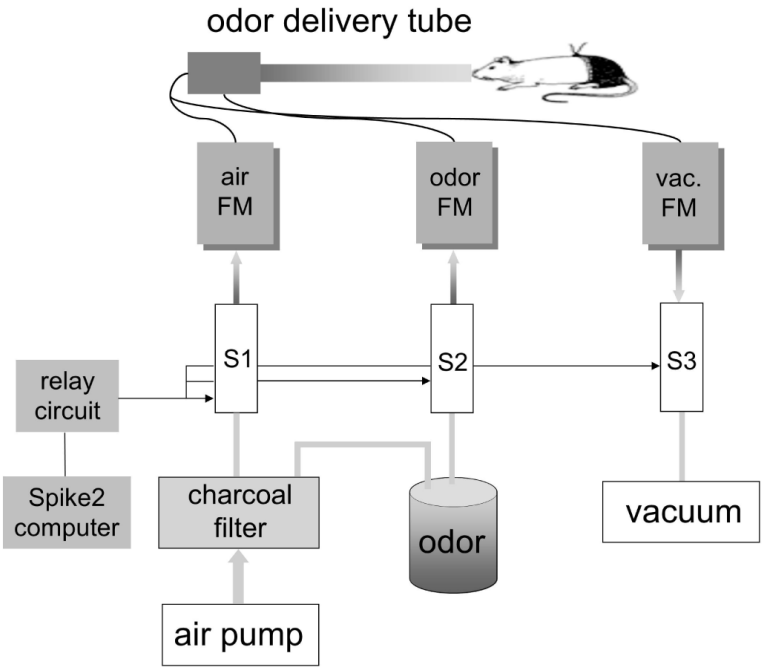

Fig. 1.

Schematic representation of the odorant delivery system. Air, driven by a pump, was purified in charcoal filter to remove spurious odorants. Fast switching solenoid valves (S1, S2, S3) were used to control airflow through flow meters (FM). The solenoids were opened/closed by a relay circuit which in turn received input from a CED unit under the control of Spike2 software. S1 was closed only under stimulation. During odorant stimulation S2 was opened, allowing filtered air to pass through the odor container and enter the delivery tube. At the end of a trial, S3 was opened to rapidly remove odor particles from the rat's vicinity.

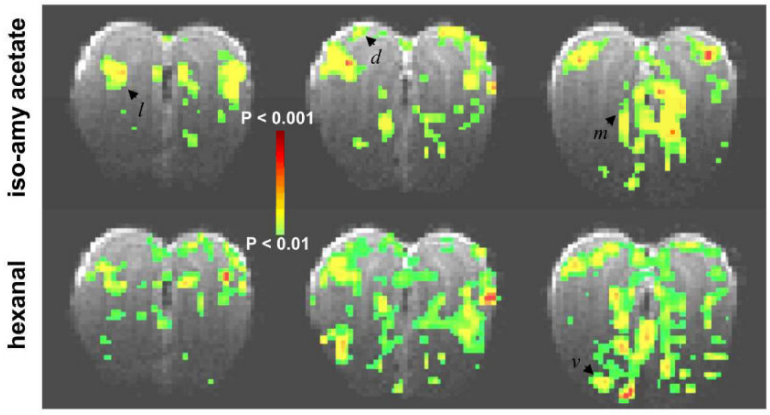

Fig. 2.

BOLD responses from the olfactory bulb in Sprague-Dawley rats. The rat was exposed to isoamyl acetate (100%) and hexanal (100%) for a duration of 60 s each. The *t* maps were generated by comparing the mean signals in a 60 s baseline period before the odorant exposure. Odor-elicited activation patterns were imaged in 10 coronal slices with 500 μm thickness, of which three slices (4–6) are shown anterior-to-posterior (left to right). Both odors elicited distributed, yet non-identical responses throughout the bulb. Dorsal (*d*), lateral (*l*), and medial (*m*), and ventral (*v*) foci are identified by arrows. All data shown are from single trial runs.

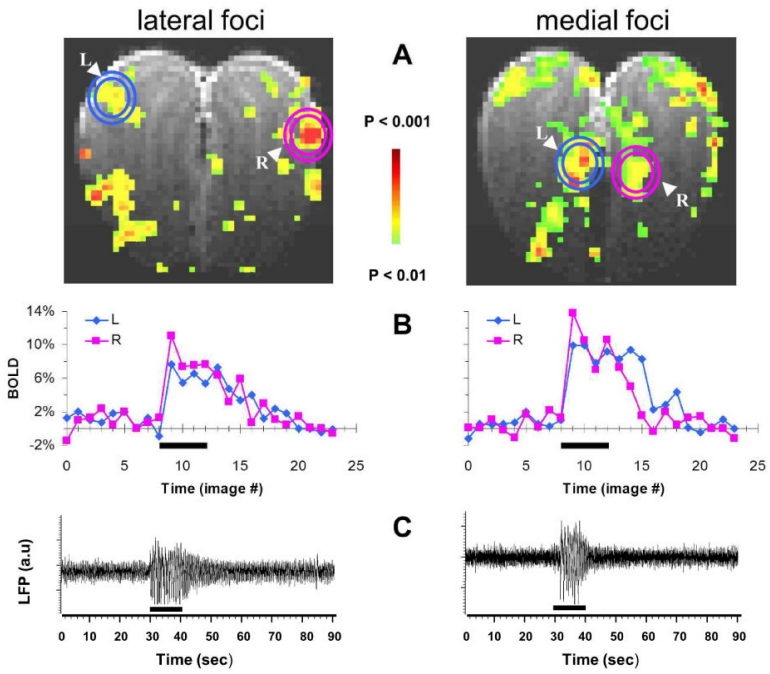

Fig. 3.

Multi-modal responses from the olfactory bulb in Sprague-Dawley rats. Lateral (left) and medial (right) responses as measured by BOLD and LFP during hexanal (100%) exposure. (A) The BOLD activation maps from slices 8 (A) and 13 (B) situated from anterior-to-posterior in one subject where the entire olfactory bulb was imaged using 20 coronal slices with 250 μm thickness. The *t* maps were generated by comparing the mean signals in a 60 s baseline epoch before the odorant exposure. The circles shown in the BOLD maps identify the lateral (left) and medial (right) foci that were probed by electrophysiology (see below). (B) The BOLD responses from the circled (L,R) regions in each slice. Comparison of the two BOLD traces in the lateral (left) and medial (right) regions depicts the inter-bulbar differences (L,R). (C) The LFP responses measured from another animal but for the same odorant and the lateral/medial areas shown above. The lateral (left) and medial (right) LFP signals were made from the left and right olfactory bulbs, respectively. The exposure periods are indicated by the black bars in the middle and bottom rows. All data shown are from single trial runs.

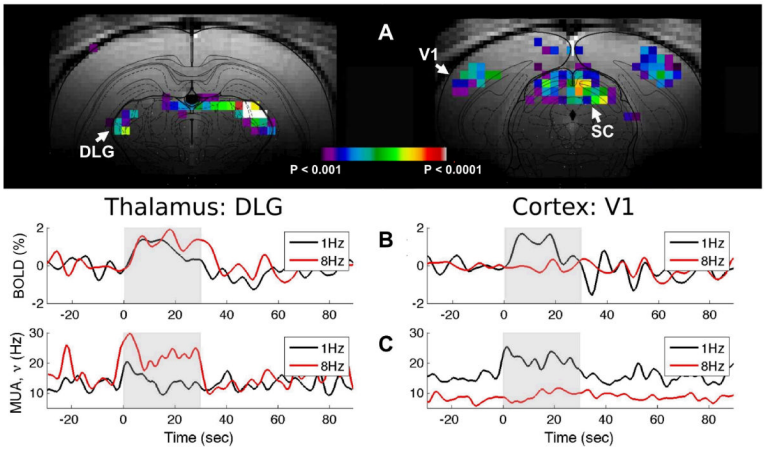

Fig. 4.

Multi-modal responses from the visual cortex during bilateral light stimulation (white; 50 ms pulses; 30 lux) in Long Evans rats. (A) Cortical and subcortical BOLD responses with 1 Hz stimulation applied for 30 s duration. Data from five trials in one animal were averaged and the *t* maps were generated by comparing the mean signals in a 30 s baseline period before the 30 s stimulation block. The MRI data were overlaid on the structural outlines from the atlas of Paxinos and Watson [53]. Bilateral responses were observed in the dorsal lateral geniculate nuclei of the thalamus (DLG; left), the primary visual cortex (V1; right), and the dorsal layers of the superior colliculus (SC; right). At higher frequencies there were weaker BOLD responses in the cortex. Results with green light were qualitatively similar to these results with white light. The time courses of (B) BOLD and (C) MUA responses to 1 Hz (black line) and 8 Hz (red line) stimuli in DLG (left) and V1 (right) from single trial runs. (B) The BOLD responses were calculated by averaging several activated voxels within a region-of-interest (in a single trial) from the maps shown above. (C) The MUA responses were obtained from another animal but under the similar experimental conditions (white; 50 ms pulses; 23 lux). The coordinates of DLG and V1 were guided by prior fMRI results: DLG: [−4.8 mm posterior, −3.8 mm lateral to bregma, −4.0 mm ventral from dura]; V1: [−5.6 posterior, −3.9 lateral to bregma, −0.9 mm ventral from dura at an angle of 10° from the vertical axis]. The 30 s stimulation period is indicated by the shaded region.

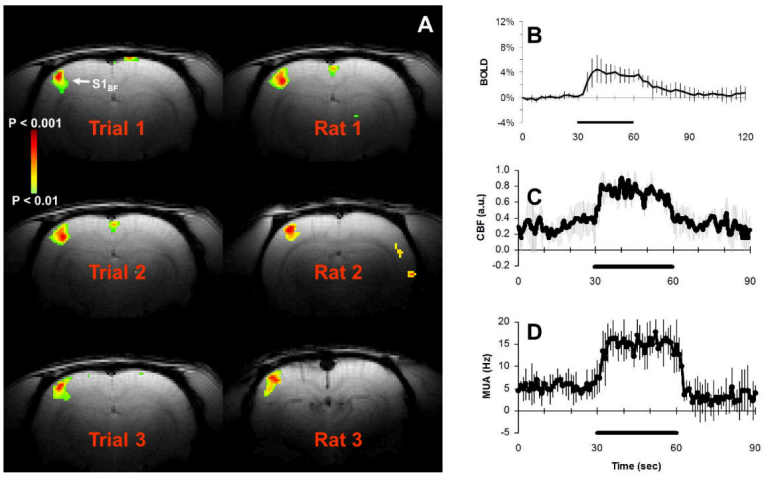

Fig. 5.

Multi-modal responses from the contralateral whisker barrel field ($S1_{BF}$) during 8 Hz whisker stimulation in Sprague-Dawley rats. (A) Reproducibility of $S1_{BF}$ BOLD activation maps in the same subject (see Trial column; left) as well as other subjects (see Rat column; right). The *t* maps were generated by comparing the mean signals in a 30 s baseline epoch before the stimulation. All data shown are from single trial runs. Averaged time courses from the $S1_{BF}$ are shown for (B) BOLD ($n = 6$), (C) CBF ($n = 5$), and (D) MUA ($n = 5$). The 30 s stimulation period is indicated by the black bar. Vertical bars or gray shading represent standard deviations from the mean.

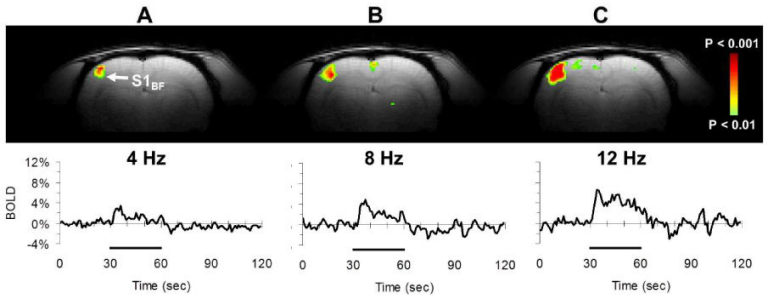

Fig. 6.

Frequency-dependent BOLD responses from the contralateral whisker barrel field ($S1_{BF}$) in Sprague-Dawley rats. The *t* maps were generated by comparing the mean signals from 30 s epochs of baseline and stimulation. In the same subject, $S1_{BF}$ BOLD responses are shown for (A) 4 Hz, (B) 8 Hz, and (C) 12 Hz whisker stimulations. The top and bottom panels show the activation maps and time courses, respectively. All data shown are from single trial runs. The 30 s stimulation period is indicated by the black bar.

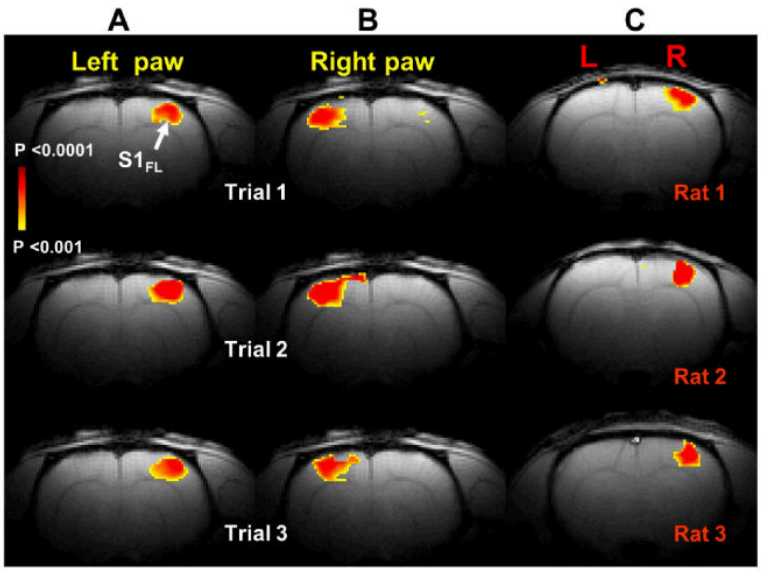

Fig. 7.

BOLD responses from the contralateral forelimb area ($S1_{FL}$) during 3 Hz forepaw stimulation (0.3 ms pulses; 2 mA) in Sprague-Dawley rats. (A) Reproducibility of $S1_{FL}$ BOLD activation maps in the same subject during left paw and right paw stimulations (see Trial column; left and middle) as well as other subjects (see Rat column; right). The *t* maps were generated by comparison of the mean signals from 30 s baseline and stimulation periods. All data shown are from single trial runs.

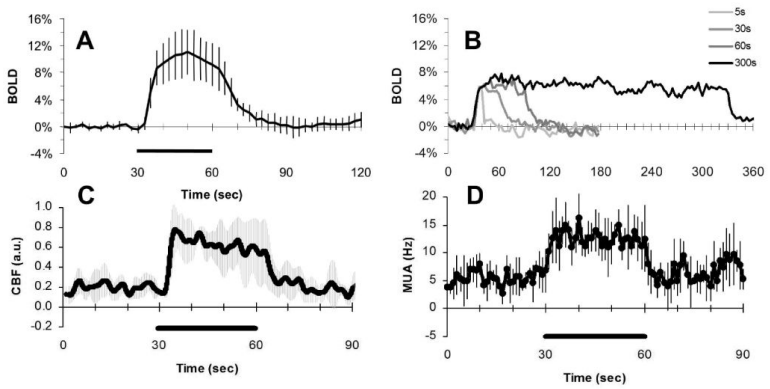

Fig. 8.

Multi-modal responses from the contralateral forelimb area ($S1_{FL}$) in Sprague-Dawley rats (0.3 ms pulses; 2 mA; 3 Hz). BOLD time courses from the $S1_{FL}$ are shown for (A) averaged during 30 s stimulation ($n = 8$) and (B) a single subject where the stimulus duration was varied (5–300 s). The averaged time courses from the $S1_{FL}$ are shown for (C) CBF ($n = 5$), and (D) MUA ($n = 5$). The stimulation period is indicated by the black bar. Vertical bars or gray shading represent standard deviations from the mean.